MEASUREMENTS OF THE DIELECTRIC PROPERTIES OF ZnS IN THE FAR INFRARED USING THz- TDS

By

LAKSHMI THAMIZHMANI

Bachelor of Science

University of Madras

Chennai, India.

2002

Submitted to the faculty of the
Graduate College of the
Oklahoma State University
in partial fulfillment of
the requirements for
the Degree of
MASTER OF SCIENCE
December, 2004

MEASUREMENTS OF THE DIELECTRIC

PROPERTIES OF ZnS IN THE FAR INFRARED

USING THz-TDS

Thesis Approved**:**

Dr. Weili Zhang
Thesis Advisor

Dr. Alan Cheville

Dr. Daniel Grischowsky

A. Gordon Emslie

Dean of the Graduate College

ACKNOWLEDGEMENTS

I would sincerely like to thank my advisor, Dr. Weili Zhang for his motivation, encouragement and constant support. He provided me with all the technical support I needed and was very understanding and patient. Without his supervision, this study would not have been possible. I would also like to express gratitude to my committee members Dr. Daniel Grischowsky and Dr. Alan Cheville for their valuable suggestions and stimulating discussions that helped me enhance my thesis.

A special note of thanks is due to the dedicated efforts of Abul K. Azad in teaching me and guiding me through the entire process very patiently and answering all the questions I had. I wish to acknowledge Jianming Dai for helping me with the setup and all others in the Ultrafast THz Optics research group for their suggestions.

Finally, I would like to thank my parents Mangalam and Thamizhmani; my brother Natrajan, grandmother Lakshmi for all the sacrifices that they have made and all my friends who gave me encouragement and love throughout the process of my study.

TABLE OF CONTENTS

Chapter **Page**

LIST OF TABLES

LIST OF FIGURES

Figure **Page**

CHAPTER I

INTRODUCTION

This thesis discusses the characterization of the frequency dependent optical and dielectric properties of ZnS in the far infrared region by THz time domain spectroscopy.

Terahertz time domain spectroscopy (THz TDS) is a technique that uses sub-picosecond pulses to study the spectroscopic properties of materials in the relatively unexplored, far infrared region. The THz radiation generated consists of a single cycle of electromagnetic radiation with an extremely broad bandwidth. The energy that each THz pulse contains is quite low but the coherent detection process in which the detector is gated with a time-delayed ultrafast pulse enables high signal-to-noise measurements. The technique is phase sensitive and helps find the real and imaginary parts of the dielectric function of the material being characterized. Ultrashort terahertz pulses are used and hence, it is possible to measure the ultrafast far-IR response of a material to an impulse perturbation.

This research was mainly motivated by the need to find potential applications of ZnS nanostructures in THz optoelectronics. Being a II- VI compound semiconductor with a wide-band gap of 3.6 eV, ZnS has optical applications in the infrared and far infrared

regions [1] and is used in displays and lasers due to its luminescent properties. It is also widely used as the base material for cathode-ray tube luminescent materials, catalysts, electroluminescent devices [2], and UV semiconductor lasers for optical lithography.

ZnS is a suitable component for the windows or lenses of infrared sensors, especially those exposed to harsh surroundings due to its optical and erosion- resistance properties. Applications as sensors include online monitoring of plants, crime prevention, and temperature measurement in microwave ovens. Equipment used for the above uses infrared radiation at a wide range of wavelengths. For the optical components that make the windows or lenses of these sensors, the potential to transmit light across a wide wavelength band or to block light of a particular wavelength band has to be increased.

ZnS has a high refractive index and a high transmittance in the visible range and is vital in the field of photonics. In window applications, the presence of an optical window made of ZnS at the entrance aperture of aerial equipment causes a reduction in the signal to noise ratio because of absorption of the signal sent to the target by the window and the addition of noise by the photons that are emitted by the window. This indicates an increase in the absorption or emission of infrared waves that is caused by lattice absorption in ZnS. This necessitates the study of the effect that the crystal structure has on the optical properties of ZnS.

ZnS nanostructures have gained a lot of attention that can be attributed to the properties arising from their size in the nanometer range [3]. Nanobelts (nanoribbons)

[4,5], nanowires [6,7], nanocables, nanorods, nanocable- aligned tetrapods, nanoparticles [8,9] and nanotubes have been synthesised. These modify electronic, mechanical, luminescent and optical properties and find applications in nanoelectronics, photonics and as tools for biomedical applications. It also has potential applications in terahertz optoelectronics. Hence the study of the characteristics and the material properties of ZnS gains further importance so as to improve our understanding of the semiconductor and expand its applications.

The characteristic properties of a material such as the refractive index, absorption coefficient and dielectric constant can be more precisely characterized using THz- TDS in the far infrared region than any other method. This justifies our choice of terahertz time domain spectroscopy to study ZnS, a technique based on the optoelectronic generation and reception of a beam comprised of subpicosecond pulses. These electromagnetic pulses can be detected with a signal to noise ratio greater than 10,000 to 1. Due to the high signal-to-noise ratio (S/N), coherent phase detection, and non-ionizing properties, THz-TDS has shown significant advantages compared to many of the far-infrared spectroscopy modalities. It has been widely used in characterizing a variety of materials including molecular vapors, semiconductors, superconductors, biomedical molecules and tissues, nanostructures and artificial metallic structures.

THz- TDS employs a THz electromagnetic beam that is used to probe the sample. The changes in the amplitude and phase of the THz beam after it comes out of the sample help determine the absorption and refractive index of the sample over a bandwidth

extending from 0.1 to 5 THz. The THz beam is obtained from a point source and is well collimated. Such a beam can be propagated without loss over long distances (of the order of meters) without suffering loss and exhibits high dynamic power ranges. The purpose of using THz- TDS is to calculate the complex dielectric constant in the bandwidth range of the THz pulses.

The absorption and refractive index of ZnS have been measured earlier using a number of techniques such as channel spectrum technique with an interferometer [1] and numerous other methods. This thesis presents an attempt to delve into the properties of ZnS using THz- TDS which has given more accurate results than any of the previous methods.

The experiments were performed using a THz- TDS system that uses a four-paraboloidal mirror configuration instead of the conventional two- mirror approach. The idea behind this modification was to obtain a tighter focus of the THz beam and to minimize the waist size of the beam.

The characterization of three different samples of ZnS using terahertz time domain spectroscopy- single crystal ZnS, polycrystalline ZnS and nanoparticles of ZnS has been attempted. Experiments were performed to measure their absorption, dispersion and complex dielectric response over the frequency range of 0.3 to 3.5 THz using terahertz time domain spectroscopy (THz-TDS). Transverse acoustic phonons at 2.2 and 2.8 THz were identified in the crystalline ZnS samples. One remarkable observation was

that of the superposition of the two difference phonons, (LO-TO) and (LA-TA) at a low frequency, 0.78 THz. The refractive index of crystalline ZnS was fit using the damped harmonic oscillator model [11, 12]. The experimental results agree well with the previous results.

CHAPTER II

TERAHERTZ TIME DOMAIN SPECTROSCOPY

2.1 THz-TDS system

THz- TDS uses photoconductive switching of the transmitter and receiver to generate and detect terahertz electromagnetic radiation. Femtosecond laser pulses are generated by a mode- locked Ti: Sapphire laser and used to generate the THz beam.

The system shown in Fig. 2-1 incorporates a terahertz transmitter, a terahertz receiver and beam focusing and collimating optics. Terahertz radiation is generated by the transmitter which is gathered by the silicon lens and collimated by a paraboloidal mirror. The THz beam is hence made highly directional after which it enters the silicon lens at the receiver end after being focused by the second paraboloidal mirror and is then incident on the receiver chip.

The THz beam is amplitude modulated by a mechanical chopper. A lock- in amplifier that is locked to the frequency of the mechanical chopper and a current amplifier are used to measure the current produced which is proportional to the amplitude of the THz electric field at the receiver.

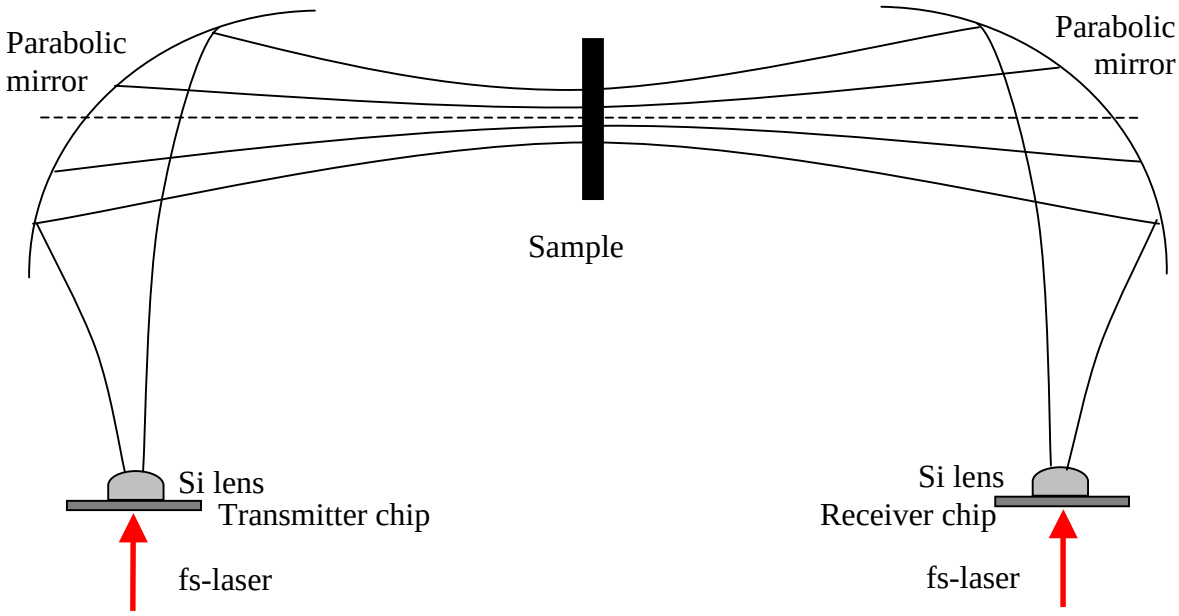

Figure 2-1: The experimental setup of the basic THz-TDS system. The sample to be characterized is placed between the two paraboloidal mirrors.

THz transmitter

Fig. 2-2 shows the basic geometry of the THz transmitter 10- 80- 10 Gallium Arsenide (GaAs) F- Chip. The coplanar transmission line structure has two Aluminium transmission lines, each 10um wide separated by a gap of 80 μm. The pattern is fabricated on the high resistivity GaAs substrate by reactive ion etching and by the deposition of the 550 nm thick Al layer on top of the 100 nm thick Ti layer by e- beam processing.

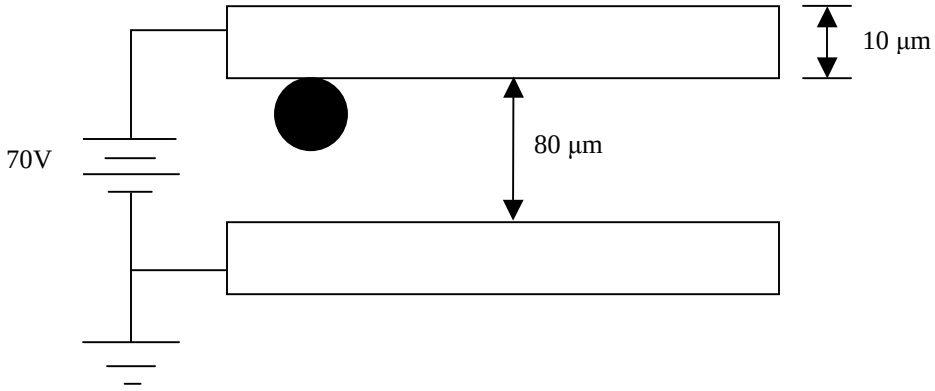

Figure 2-2: THz transmitter with the 10 μm wide antenna lines separated by 80 μm and biased at 70 V.

The chip is biased with a DC voltage of 70 volts. Femtosecond pulses are incident on the photoconductive gap in the transmitter chip making it conductive. This generates free carriers that are emitted in the form of a conical THz beam that is collimated by the silicon lens.

THz Receiver

Fig. 2-3 shows the basic geometry of a THz receiver 5- 10- 5 SOS (silicon on sapphire) Max 1 chip. The coplanar transmission line structure consists of two Aluminium lines, each 5 µm wide separated by a gap of 10 µm fabricated on a SOS substrate.

An Al layer with a thickness of 500 nm is deposited atop the 100-nm-thick Ti layer by thermal evaporation.

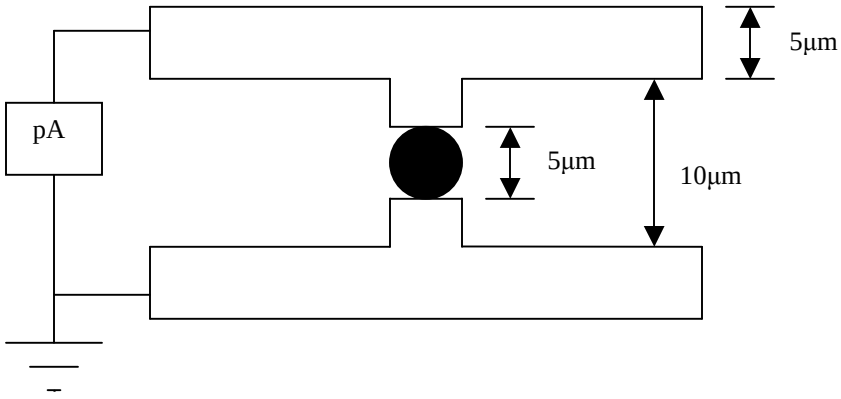

Figure 2-3: THz receiver with 5µm wide antenna lines connected to a current amplifier and separated by 10 µm. The antenna gap is 5 µm.

The silicon lens on the receiver side focuses the THz radiation. When the 5µm gap on the receiver chip is illuminated with laser pulses, the electric field of the incident beam creates a transient bias across it. The current thus produced is measured by the low noise current amplifier that is directly connected to the receiver chip.

2.2 Focused beam THz-TDS system

The modified setup as shown in Fig.2-4 was used to carry out my experiments. The setup uses four paraboloidal mirrors that are arranged in an 8F confocal arrangement. The Gaussian THz beam from the silicon lens is collimated into a parallel beam by M4 and attains a minimum waist between M2 and M3. It is recollimated after leaving M3 and focused into the silicon lens at the receiver end by M1.

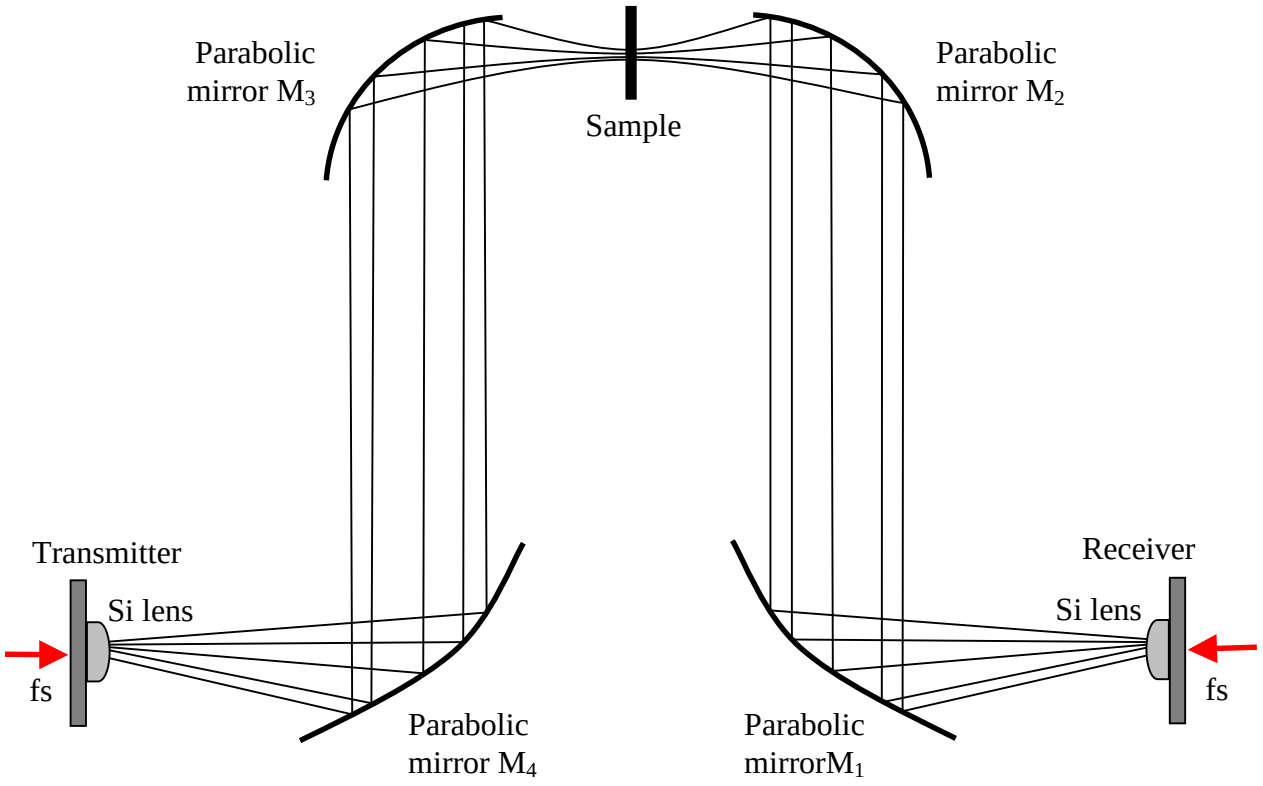

Figure 2-4: Modified THz-TDS setup using an 8F confocal geometry. The sample to be characterized is placed at the minimum waist position.

2.3 Waist calculation of propagating Gaussian beam

The ABCD law of Gaussian beam propagation describes how the radius of curvature of a spherical wave propagating in free space is transformed by an optical system [13]. The minimum waist point is located using the transmission matrix for the optical system shown in figure 2-4.

The overall transmission matrix of the system is

$$\begin{pmatrix} A & B \\ C & D \end{pmatrix} = \begin{pmatrix} 1 & d_4 \\ 0 & 1 \end{pmatrix} \begin{pmatrix} 1 & 0 \\ -1/f_4 & 1 \end{pmatrix} \begin{pmatrix} 1 & d_3 \\ 0 & 1 \end{pmatrix} \begin{pmatrix} 1 & 0 \\ -1/f_3 & 1 \end{pmatrix} \begin{pmatrix} 1 & d_2 \\ 0 & 1 \end{pmatrix} \begin{pmatrix} 1 & 0 \\ -1/f_2 & 1 \end{pmatrix} \begin{pmatrix} 1 & d_1 \\ 0 & 1 \end{pmatrix} \begin{pmatrix} 1 & 0 \\ -1/f_1 & 1 \end{pmatrix} \begin{pmatrix} 1 & d_0 \\ 0 & 1 \end{pmatrix}$$

where d_0, d_1, d_2, d_3 and d_4 are the distances from the silicon lens of the receiver to M1, between M1 and M2, between M2 and M3, between M3 and M4, from M4 to the silicon lens of the transmitter respectively.

This equation can be solved to arrive at the waist of the beam at any position in the system. From the graph in Fig. 2-5 we can observe that the minimum waist occurs midway between M2 and M3. This is where the sample should be placed for maximum beam coupling.

The beam is approximated to be Gaussian and the paraboloidal mirrors are assumed to be similar to lenses for the purpose of calculations. The minimum waist is obtained only if the illustrated setup is used with the distances as calculated.

The minimum waist that is obtained using this setup (3.5 mm) is lesser than that obtained with the 4F confocal system (25 mm). The new setup thus offers the advantages of a tighter, more focused beam as compared to that obtained from the previous setup. Figure 2-6 shows the measured reference THz pulse and its amplitude spectrum with this 8F THz-TDS system.

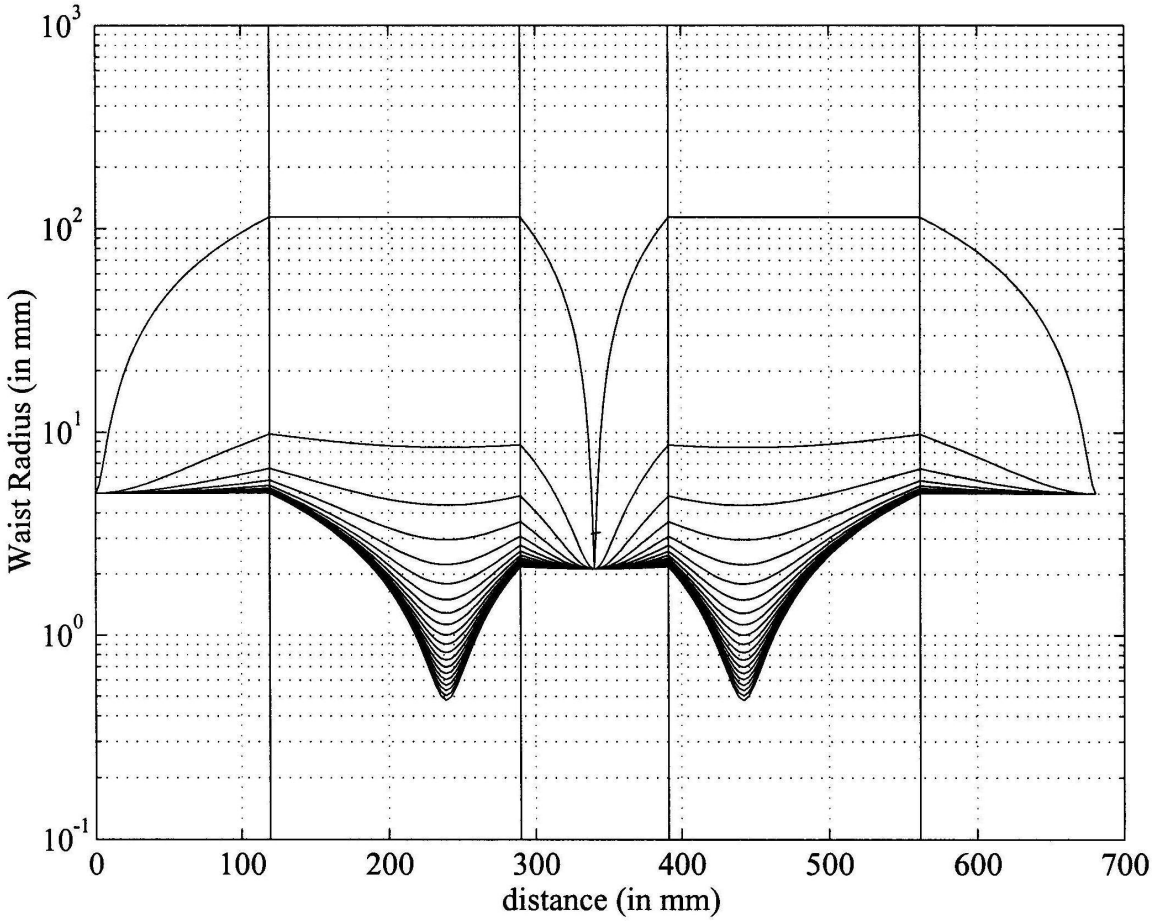

Figure 2-5: Gaussian Beam waist calculated for the 8F confocal, paraboloidal mirror system.

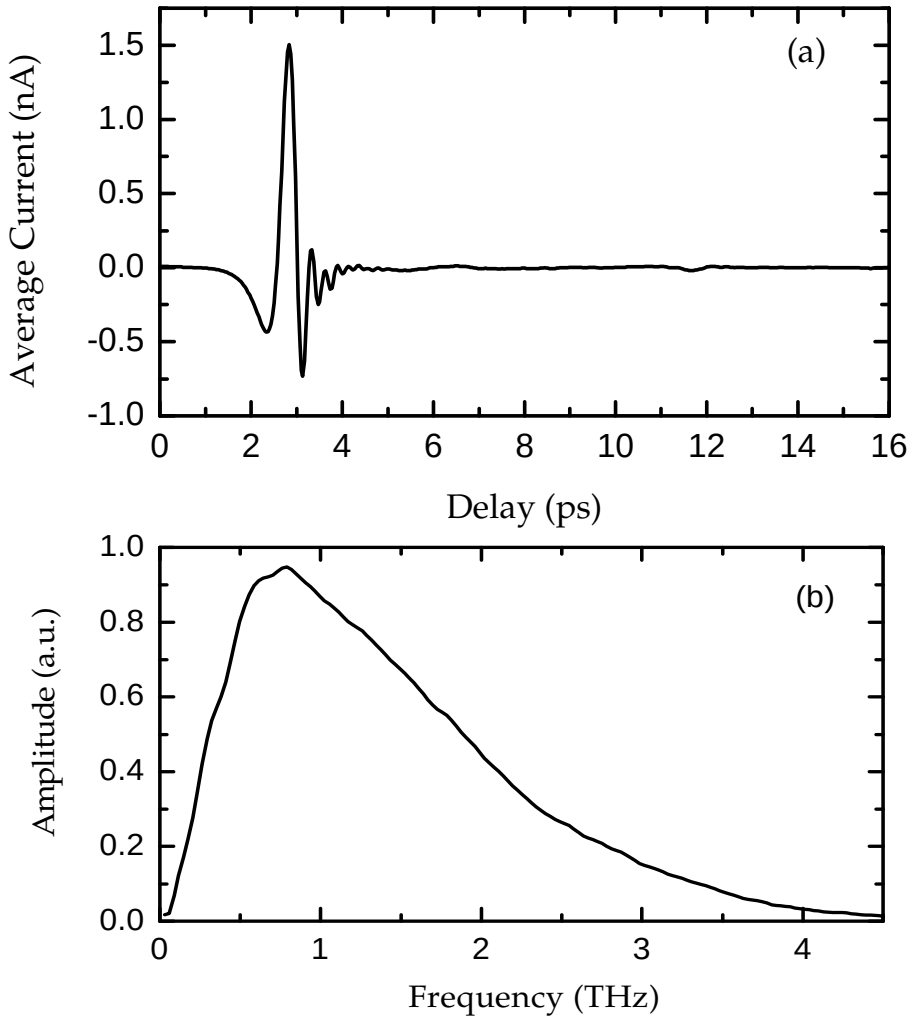

Figure 2-6 (a) Measured reference terahertz pulse propagating through air. (b) The corresponding amplitude spectrum of the reference pulse.

2.4 THz-TDS data analysis

Samples are characterized using this setup using the following procedure. Calculations reveal that the THz beam has a minimum size midway between the two paraboloidal mirrors. The sample to be studied is placed at this point so that all of the THz radiation is focused onto the sample. The amplitude of the THz beam with the sample in place is measured at the receiver and is called E_{sample} (t). The sample is removed and the amplitude of the THz pulse is measured. This is called $E_{reference}$ (t). The measured sample pulse is observed to be delayed with respect to the reference pulse and altered in shape due to the frequency- dependent absorption and surface reflections from the sample. Its peak amplitude is also reduced. The reference and sample pulses in the time domain are Fourier transformed to obtain their complex amplitude spectra, $E_{reference}$ (ω) and E_{sample} (ω) respectively. The ratio of the sample spectrum to the reference spectrum yields data about the absorption of the terahertz beam by the sample and the phase shift due to the delay caused by the increased optical path length (because the refractive index of the sample is greater than that of the surrounding medium, air). The sample has a complex refractive index indicated by

$$n(\omega) = n_r(\omega) + i\, n_i(\omega) \tag{2-1}$$

The absorption by the sample α, is related to the imaginary part of the refractive index n_i by $\alpha = 2\omega\, n_i(\omega)/c$ and the phase shift β is related to the real part of the refractive index by $\beta = 2\pi n_r L/\lambda_0$. α and β are determined from the ratio[14]

$$\frac{E_{sample}(\omega)}{E_{reference}(\omega)} = \frac{t_{12}t_{21}\exp(-\alpha L/2)\exp(i2kL)}{1 + r_{12}r_{21}\exp(-\alpha L/2)\exp(i2kL)} \quad (2\text{-}2)$$

where 'L' is the thickness of the sample through which the beam propagates and t_{12} and t_{21} are the Fresnel transmission coefficients for the beam propagating from medium 1 to medium 2 and from 2 back into 1 respectively.

The stability of the laser is important in determining the accuracy of the results as a change in the direction of the beam can lead to faulty scans. The laser used has been observed to be stable and the mode- locked pulse obtained is also good. The chopper chops the THz beam and not the laser beam. Hence the noise introduced into the system is minimized. Damages on the surface of the SOS substrate in the chip and alignment problems with the system can bring in noise. But these have been taken care of.

CHAPTER III

STUDY OF ZnS

Using THz-TDS, it is observed that the absorption in crystalline ZnS is characterized by difference ((LO-TO) and (LA-TA)) and transverse acoustic (TA) phonons centered at 0.78 THz and 2.20 THz respectively. An additional higher-frequency phonon line is observed at 2.8 THz for single crystal ZnS. These phonons account for the increased absorption as indicated by the resonance peaks in the spectra. The behavior of the index of refraction is determined by the transverse optical (TO) phonon line centered at 8.13 THz and is well fit by the relation for the dielectric response of the damped harmonic oscillator [11].

The peaks observed in the absorption spectrum of ZnS are due to singularities that arise from critical points in the Brillouin zone each of which characterize a phonon branch. These can be accounted for by four characteristic phonon energies belonging to four branches – TA, LA, TO and LO at the zone boundary. When an infrared photon interacts with lattice vibrations, energy and wave vector are conserved. TA and LA imply the transverse and longitudinal acoustic phonons at the various critical points L, X, W and Σ while TO and LO imply the transverse and longitudinal optical phonons [15].

3.1 Previous study

Considerable work in the past has been done in assigning phonons to ZnS. The following paragraphs list some of the work done on characterizing ZnS in the past.

Slack and Roberts [16] have studied absorption in the far- infrared region by single crystals of ZnS. The absorption peaks in the spectrum correspond to the simultaneous generation of multiphonons (acoustic) at critical points. They infer that acoustic phonon energies in ZnS obtained from infrared absorption, spectral emittance, X- ray scattering and neutron scattering specify the presence of a TA(L) phonon at 73 cm^{-1} (2.2 THz) and a TA(X) phonon at 93 cm^{-1} (2.8 THz). These were the best measured values obtained from [25].

Vagelatos et al. [17] have reported phonon dispersion measurements and neutron scattering data for II- VI zinc blende crystals and have assigned the TA phonons for ZnS at 0.8±0.02 THz and at 2.69± 0.04 THz respectively. The phonon dispersion curves were obtained by conducting the experiments under room temperature and using a ZnS natural crystal.

Deutsch's (1962) interpretation of the infrared data has been said to be not unique and Johnson's interpretation (1965) of Deutsch's data is also ambiguous.

Marshall and Mitra [15] have obtained the transmission spectrum of hexagonal ZnS and assigned the maximum absorption point to multiphonon combinations in ZnS of which two phonon frequencies are of interest to us (TA_1= 92 cm^{-1} (2.8 THz) and TA_2= 73 cm^{-1} (2.2 THz)). They have also predicted a TA phonon at 93 cm^{-1} for cubic ZnS which is only slightly different from the previous result and conjectured that by using very thin crystals, it would be possible to decipher the structure in the absorption spectrum of ZnS which would help assign phonon frequencies accurately. Marshall and Mitra have assigned lower values for the acoustic branch phonons in ZnS as compared to Deutsch's previous work on the same.

Brafman and Mitra [18] have studied the Raman spectra of wurtzite and zinc blende type ZnS single crystals by exciting them by a He- Ne laser source at 6328 Å and an argon- ion laser at 4880 and 5145 Å and have assigned a phonon branch at 72 cm^{-1} (2.2 THz) for the wurtzite- type ZnS crystal and have also claimed that earlier work on the Raman spectrum of hexagonal ZnS by Poulet, Klee and Mathien [20] is incomplete. A complete study of the Raman effect in hexagonal ZnS had not been possible then and they have attributed it to the non- availability of symmetric, high- quality ZnS crystals.

Schneider and Kirby [20] have measured the Raman spectra of 2H and 4H polytypes of wurtzite ZnS. They have observed the TA (L)- E_2 phonon at 69.2 cm^{-1} and the TA (L)- E_1 phonon at 69.6 cm^{-1} at room temperature.

W. G. Nilsen [21] has performed a detailed study on the second- order Raman effect in cubic ZnS and has predicted a TA phonon at 88 cm^{-1} and an LA phonon at 110 cm^{-1} assuming that the scattering came from the X and L critical points of the Brillouin zone. The superposition of the two difference phonons, (LO-TO) and (LA-TA) is also predicted at 0.78 THz.

Irwin [22] has arrived at phonon frequencies for cubic ZnS in the infrared region and using the second neighbor ionic model has predicted TA phonons at 96cm^{-1} (2.9 THz) and at 65 cm^{-1} (1.97 THz).

Hattori et al. [1] have measured the indices of refraction of ZnS in the spectral region from 10 to 100 cm^{-1} and described them using the dispersion formula of an undamped harmonic oscillator.

Klein and Donadio [23] have reported critical point mode frequencies for cubic ZnS at room temperature and compared their results with neutron scattering data. Chemically vapor deposited ZnS was used to study the infrared absorption spectrum of cubic ZnS and found to obey Raman's spectral results. The absorption spectrum is described using the TA(X) and the TA (L) phonons at 88± 1 cm^{-1} (2.6-2.7 THz) and 72± 1 cm^{-1} (2.2 THz). The experiments were done using thick samples of ZnS obtained by chemical vapor deposition that had previously been unavailable. Their interpretation of the results show that in the two- phonon region, the magnitude of the total absorption and its frequency dependence derive from the product of three contributions- the probability

of an interaction between a photon and a phonon, the strength of the coupling mechanism, the two- phonon density of states that gives structure to the absorption spectrum [23].

3.2 THz-TDS Experiments

3.2.1 Characterization of single crystal ZnS

The single crystal ZnS used in this study is an undoped, 10 mm × 10 mm × 1-mm-thick, <100> freestanding crystal optically polished on both sides (RMT Ltd, Russia). It was grown from a source of polycrystalline ZnS at temperature of 1100 – 1250 ºC and a pressure of 1 atmospherein a hydrogen -filled ampoule using the seeded vapor-phase free growth technology [24]. Growth was along the <111> direction and the crystal consists of 96 - 98% zinc blende structure and only 2- 4% Wurtzite structure. The resistivity of the crystal is in the range of 10^8 to 10^{12} ohm cm.

The experiments were carried out at room temperature using standard THz-TDS transmission measurements. A self-mode-locked Ti: sapphire laser capable of generating 26-fs, 88-MHz optical pulses was used as the excitation source. Both the terahertz transmitter and receiver chips were driven by 10-mW femtosecond pulses for the generation and detection of up to 4.5-THz broadband electrical pulses. The 8-F confocal geometry ensures excellent beam coupling between the transmitter and receiver and compresses the terahertz beam to a diameter of 3.5 mm which is small compared to the size of the ZnS sample, enabling complete coupling of all the frequency components of the beam into the sample. The terahertz system is placed in an enclosure purged with dry air to eliminate the absorption of terahertz wave by water vapor. The sample is attached to an aluminum holder and centered over a 4.5-mm-diameter hole in the plate, which

defines the optical aperture. Another identical clear hole is used to take reference signal designated as the input pulse.

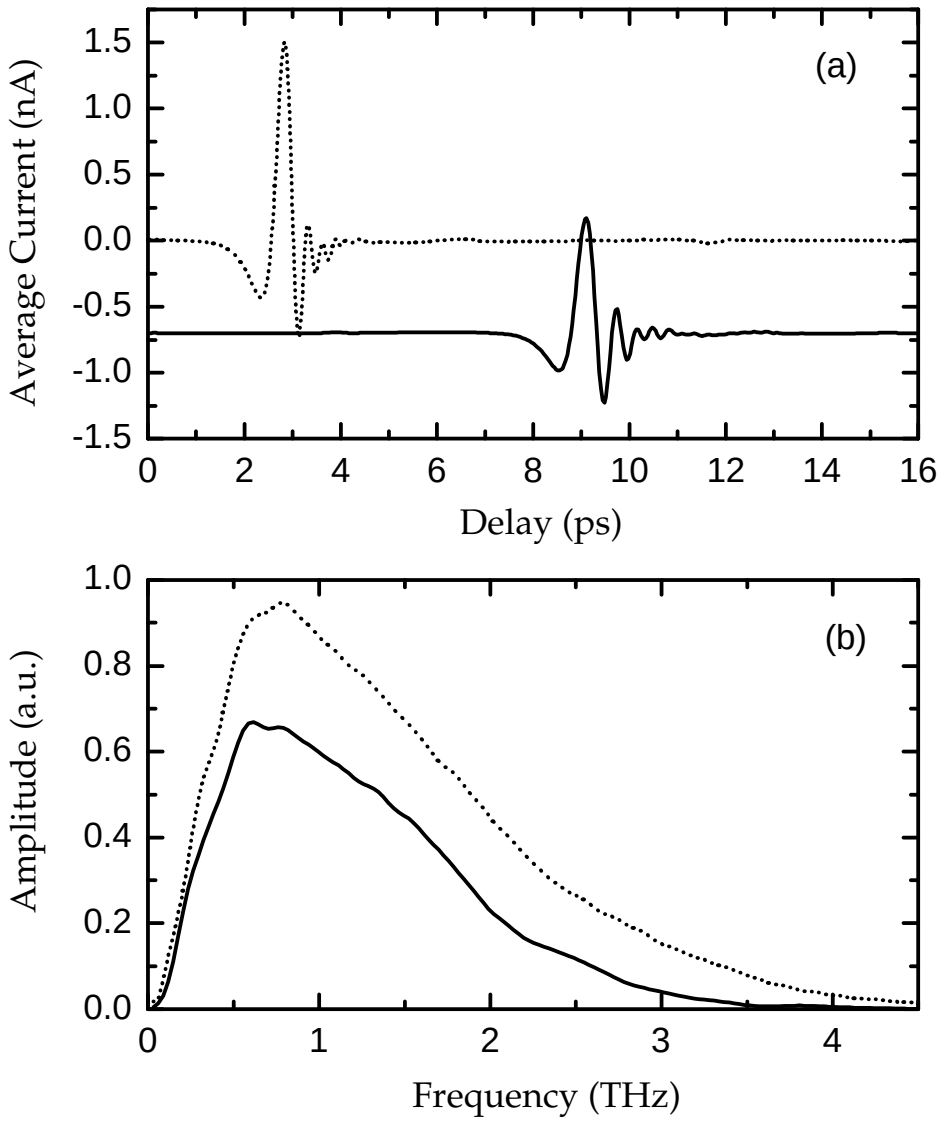

Figure 3-1 (a) Measured reference terahertz pulse (dotted line) and the output terahertz pulse (solid line, offset by - 0.7 nA for clarity) for single crystal ZnS. (b) The corresponding amplitude spectra of reference pulse (dotted line) and output pulse (solid line).

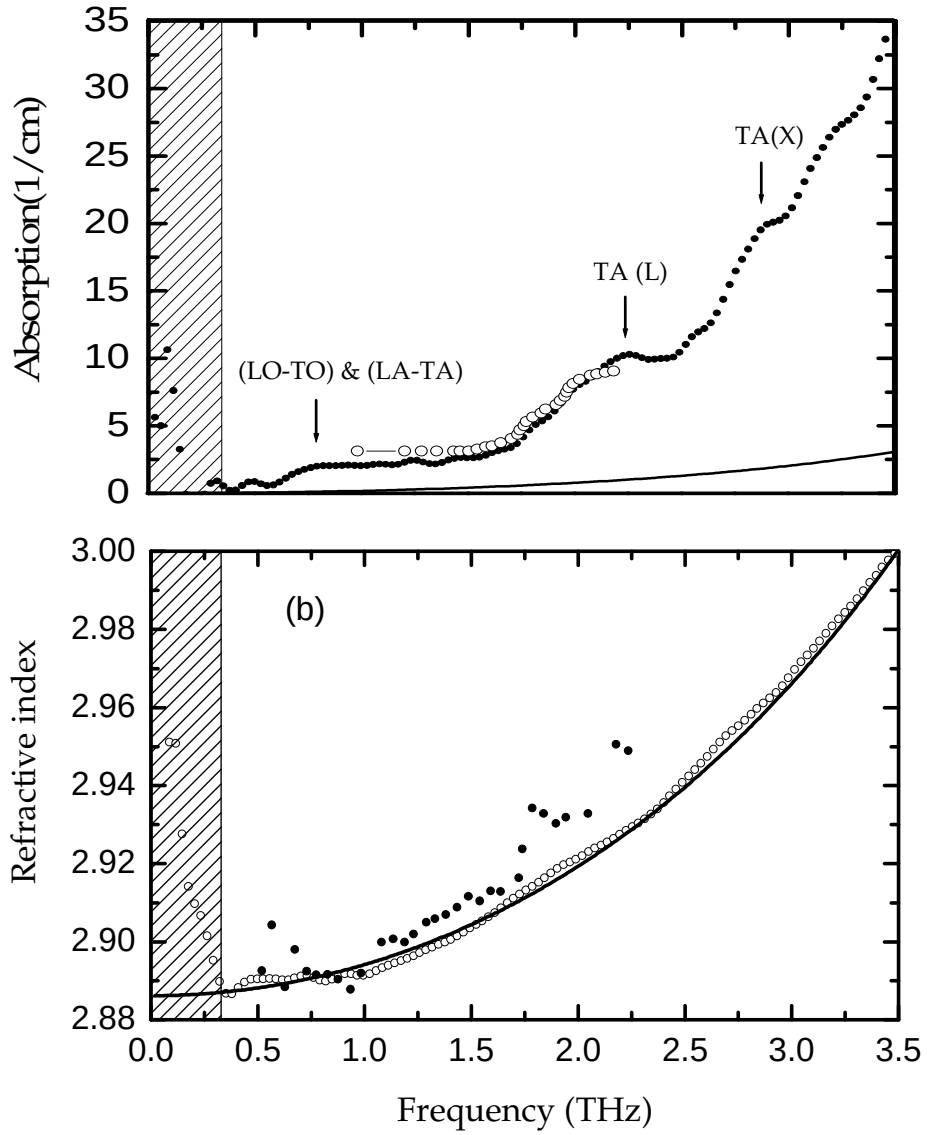

Figure 3-2 (a) Comparison of measured results (open circles) for the absorption of single crystal ZnS with data from [1] (dots) and from theoretical calculations (solid line) (b) Comparison of measured (open circles) refractive index of single crystal ZnS with: values calculated using the damped harmonic oscillator model (solid line) and the data from [1] (dots).

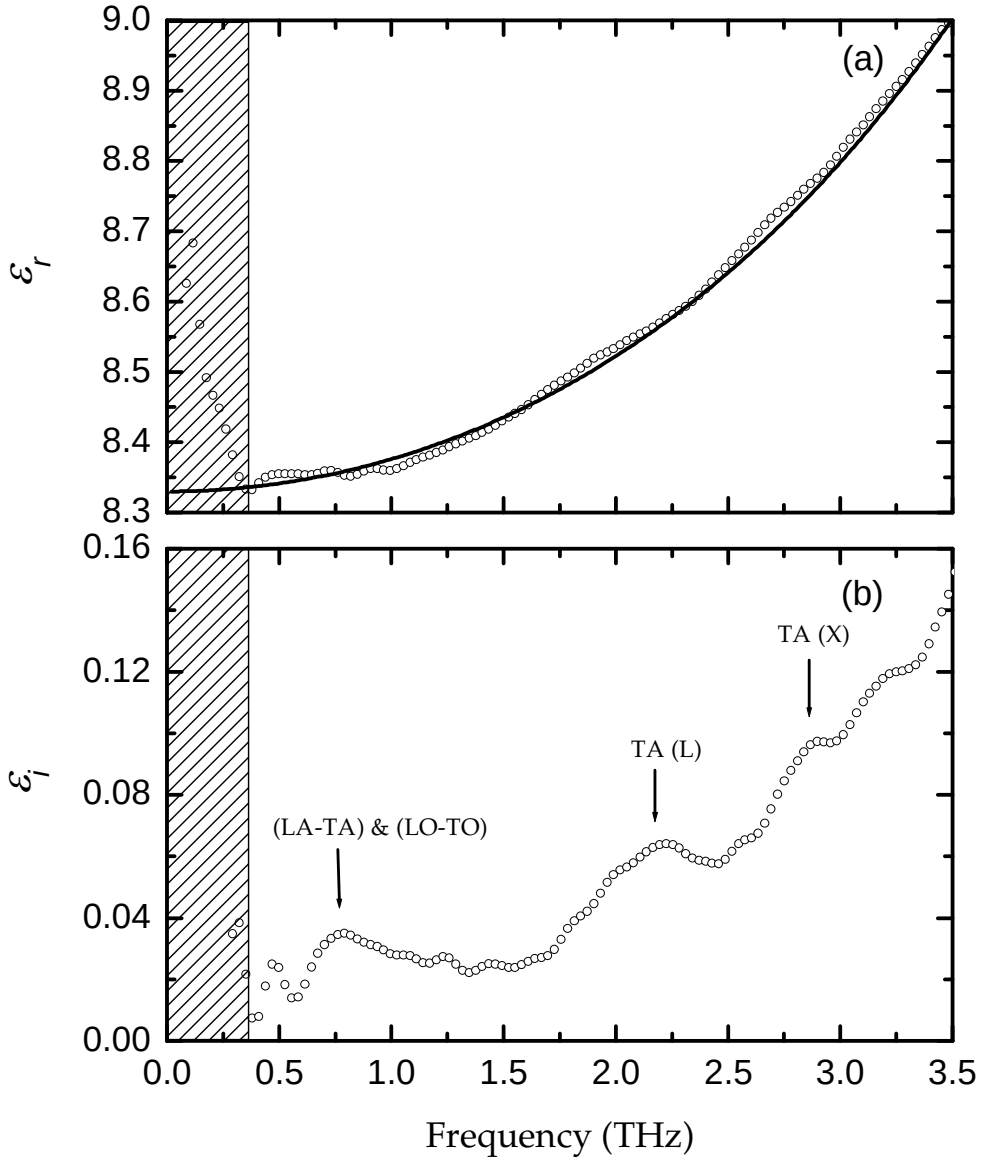

Figure 3-3: Complex dielectric constant of single crystal ZnS: (a) measured real part of dielectric constant ε_r (open circles) and the theoretical fitting (solid line); (b) measured imaginary dielectric constant ε_i.

3.2.2 Interpretation of THz-TDS results

The measured terahertz pulses transmitted through the single crystal ZnS and reference and the corresponding Fourier transform amplitude spectra are shown in Fig. 3-1. In order to increase the S/N, seven individual measurements were averaged to obtain the curve of each pulse. The peak amplitude of the sample spectrum is reduced by about 30% due to the frequency-dependent absorption and reflection of the ZnS sample. The frequency-dependent coefficient of power absorption for single crystal ZnS is extracted from the experimental data using the well-known amplitude transmission function of a parallel dielectric slab [14]. Because of the relatively clean separation in time between the main transmitted pulse and the first internal reflection, the data analysis was performed on the main pulse only. The complex spectrum of the transmitted pulse $E_0(\omega)$ is determined by the product of the input spectrum $E_i(\omega)$ and the total transmission function of the sample where

$$\frac{E_0(\omega)}{Ei(\omega)} = t_{12}t_{21}exp(ikL)exp(-\alpha L/2) \tag{3-1}$$

$$E_i(\omega) = E_R(\omega)exp(ik_0L); \tag{3-2}$$

$E_R(\omega)$ is the reference spectrum and the phase correction k_0L is due to the free-space occupied by the sample; t_{12} and t_{21} are the frequency-dependent complex Fresnel transmission coefficients; α is the power absorption coefficient, k is the sample wavevector, $k = 2\pi n/\lambda_0$, and L is the sample thickness. For this simple case, the denominator in the complex amplitude transmission function for the parallel

dielectric slab reduces to unity and the frequency spectrum of only the first transmitted pulse shows no oscillation [14]. This approximation enables the determination of the power absorption, α and the index of refraction, n of the sample quite accurately [24].

The formula for the dielectric constant of an undamped harmonic oscillator as mentioned in Hattori's paper is erroneous [1] and the corrected version is shown below. The corrected formula for the dielectric constant ε (υ) at a frequency 'υ' is

$$\varepsilon(\upsilon) = \frac{\varepsilon_0 \upsilon_{TO}^{\,2} - \varepsilon_\infty \upsilon^2}{\upsilon_{TO}^{\,2} - \upsilon^2} \qquad (3\text{-}3)$$

which replaces the incorrect 'ε' term in the denominator as mentioned in [1] with 'υ'. However, the more accurate, damped harmonic oscillator model is used in our analysis.

The experimentally extracted power absorption of single crystal ZnS is plotted in Fig. 3-2 (a). Three resonance lines are observed at 0.78 THz, 2.20 THz and 2.80 THz respectively, which are in good agreement with the previous prediction or observation as the superposition of the difference phonons, ((LO-TO) and (LA-TA)), TA(L) and TA(X) phonons respectively[1, 16, 25, 23, 17]. The first resonance peak centered at 0.78 THz has lifted the absorption coefficient to 2 cm^{-1}. This is interpreted as the superposition of the two difference bands (LO-TO) and (LA-TA). This difference combination band at an energy shift of 28 cm^{-1} is made up of the following frequencies: TA = 88 cm^{-1}, LA = 110

cm^{-1}, TO = 306 cm^{-1} and LO = 333 cm^{-1}[21]. The second and broad resonance line with a peak power absorption coefficient of 11 cm^{-1} is located at 2.20 THz. It is referred to as the transverse TA (L) phonon connecting to two-phonon generation processes of acoustic phonons [18] and was verified with neutron scattering measurements [17]. The resonance feature at 2.80 THz showing peak absorption of 20 cm^{-1} was previously observed to be one of the critical-point mode frequencies by neutron scattering measurements at room temperature [17]. It was defined as the TA (X) phonon and was considered as one of the four characteristic zone-boundary phonons used to describe the three-phonon processes in cubic ZnS [25]. In comparison with previous measurements the dots show the room temperature absorption data in the frequency range of 1.0 – 2.2 THz by channel spectrum technique [1] and the theoretically calculated absorption. The not-so-good power absorption fit to the TO-phonon line at 8.13 THz, as shown by the solid line in Figure 3-2 (a) however, shows a very weak effect compared to the observed TA-phonon resonance features that dominate at 2.2 and 2.8 THz as well as the LA phonons around 5.80 THz [17].

Figure 3-2 (b) shows the frequency-dependent refractive index of single crystal ZnS. The measured result represented by open circles also reveals the effect of the resonance lines of the TA (L) phonon at 2.20 THz and the TA (X) phonon at 2.80 THz. The refractive index increases with increasing frequency [11]. This feature is dominated by a high-frequency TO-phonon resonance as predicted in early work [1]. However, the increase in the refractive index of ZnS is not very sharp since the TO-phonon line is centered at 8.13 THz which is high. The measured refractive index is then theoretically

fitted using the dielectric response of a damped harmonic oscillator [11, 12]. The frequency-dependent dielectric constant in the infrared region for the harmonic oscillator is formulated as [11, 12]

$$\varepsilon(\omega) = \varepsilon_\infty + \frac{\varepsilon_{st}\omega_{TO}^2}{\left(\omega_{TO}^2 - \omega^2 + 2i\gamma\omega\right)} \tag{3-4}$$

where ω_{TO} is the transverse optical (TO) phonon frequency, ε_∞ is the optical dielectric constant, ε_{st} describes the strength of the TO-phonon resonance at $\omega_{TO}/2\pi$, $\varepsilon_\infty + \varepsilon_{st} = \varepsilon_0$ is the static dielectric constant and γ is the damping coefficient. The frequency dependent complex dielectric constant is also given by the square of the complex refractive index

$$n^2 = (n_r + in_i)^2 = \varepsilon(\omega) \tag{3-5}$$

The imaginary part of the index, n_i can be obtained from $n_i = \alpha\lambda_0/4\pi$ where α is the power absorption coefficient and λ_0 is the free-space wavelength. The solid line in Fig. 3-2 (b) shows the theoretical fitting of the measured index *n* with the TO-phonon resonance centered at $\omega_{TO}/2\pi = 8.13\,\text{THz}$ with a linewidth of $\gamma/2\pi = 0.025\,\text{THz}$, optical dielectric constant, $\varepsilon_\infty = 5.13$, and the TO-phonon strength $\varepsilon_{st} = 3.19$. The good agreement between the measured data and fitting verifies the dominance of the TO-phonon resonance on the refractive index of ZnS. The absorption curve obtained from the theoretical calculations however, rises with an increase in the value of linewidth. The refractive index of ZnS at various temperatures in the range of 19 – 100 cm^{-1} has been studied previously by using channel spectrum technique [1]. The previous data at room

temperature has been plotted by dots for comparison. It was fit with an undamped harmonic oscillator using parameters $\omega_{TO}/2\pi = 7.80\,\text{THz}, \varepsilon_\infty = 4.7$ and $\varepsilon_0 = \varepsilon_\infty + \varepsilon_{st} = 8.34$ [1]. My results show a better correlation with the theoretical fit and demonstrate the efficiency of the THz-TDS characterizations and the accuracy with which it can determine the optical and dielectric parameters of the measured sample.

Based on the measured data of power absorption and refractive index the frequency-dependent complex dielectric function of single crystal ZnS was extracted as shown in Fig.3-3. The real and imaginary part of the dielectric constant are determined as

$$\varepsilon_r = n_r^2 - n_i^2 = n_r^2 - \left(\alpha\lambda_0/4\pi\right)^2 , \tag{3-6}$$

$$\varepsilon_i = 2n_r n_i = \alpha n_r \lambda_0/2\pi \tag{3-7}$$

In Fig. 3-3 (a), the real dielectric constant shows a feature which is essentially the square of the refractive index n_r. This is because the absorption by the sample is small in the spectral region concerned and the contribution of the absorption coefficient to the real dielectric constant is nearly negligible. The plot of the imaginary dielectric constant showed in Fig. 3-3 (b) has features similar to the power absorption curve but reveals the phonon resonance peaks more clearly. It therefore provides further verification of the TA-phonon resonances determined previously by the power absorption and refractive index.

3.2.3 Characterization of polycrystalline ZnS

The polycrystalline ZnS sample (Crystan Ltd., United Kingdom) is a 25.4 mm × 25.4 mm × 3.42-mm-thick, double-side pulsed slab. It was synthesized from zinc vapor and gaseous hydrogen sulphide, and formed as sheets on graphite susceptors.

The procedure for the characterization of polycrystalline ZnS is essentially the same as that for single crystal ZnS sample as outlined earlier in this section.

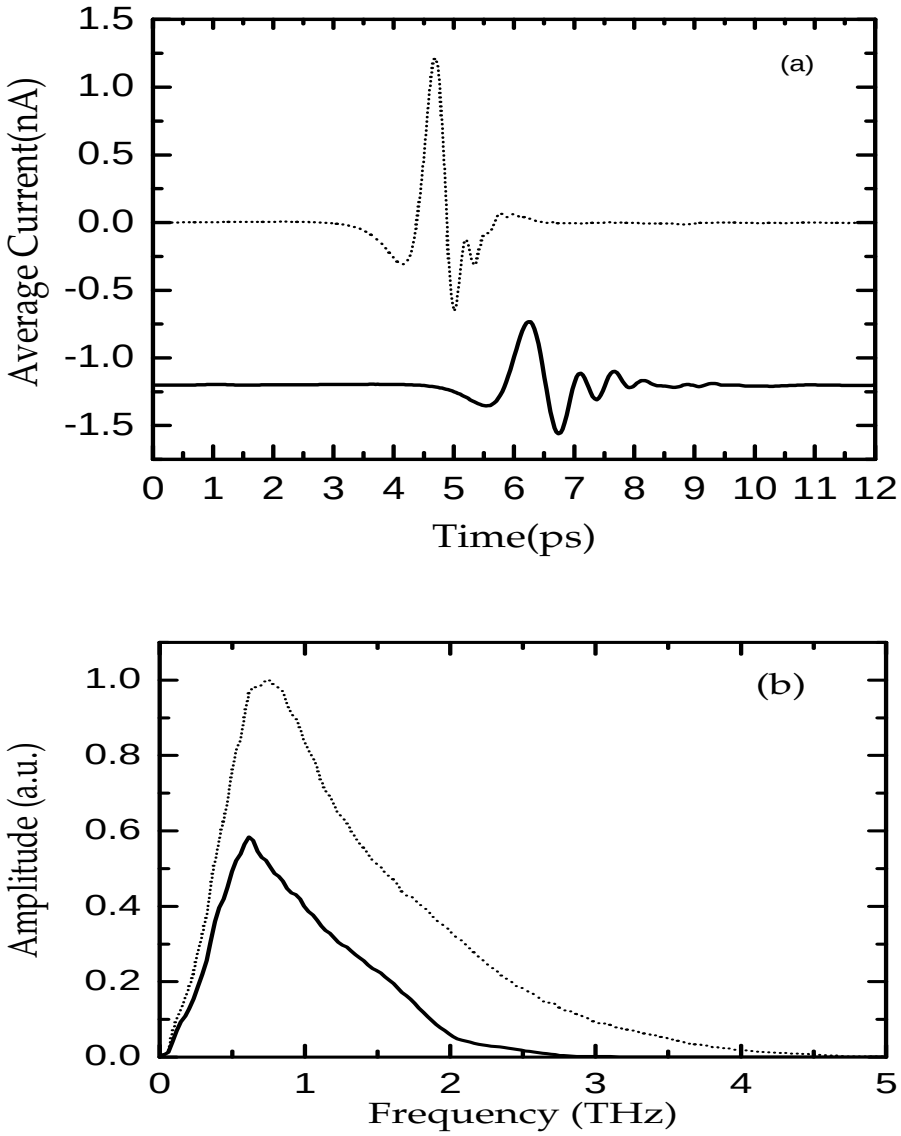

Figure 3-4 (a) Measured reference terahertz pulse (dotted line) and the output terahertz pulse (solid line, offset by – 1.18 nA for clarity) for polycrystalline ZnS. (b) The corresponding amplitude spectra of reference pulse (dotted line) and output pulse (solid line).

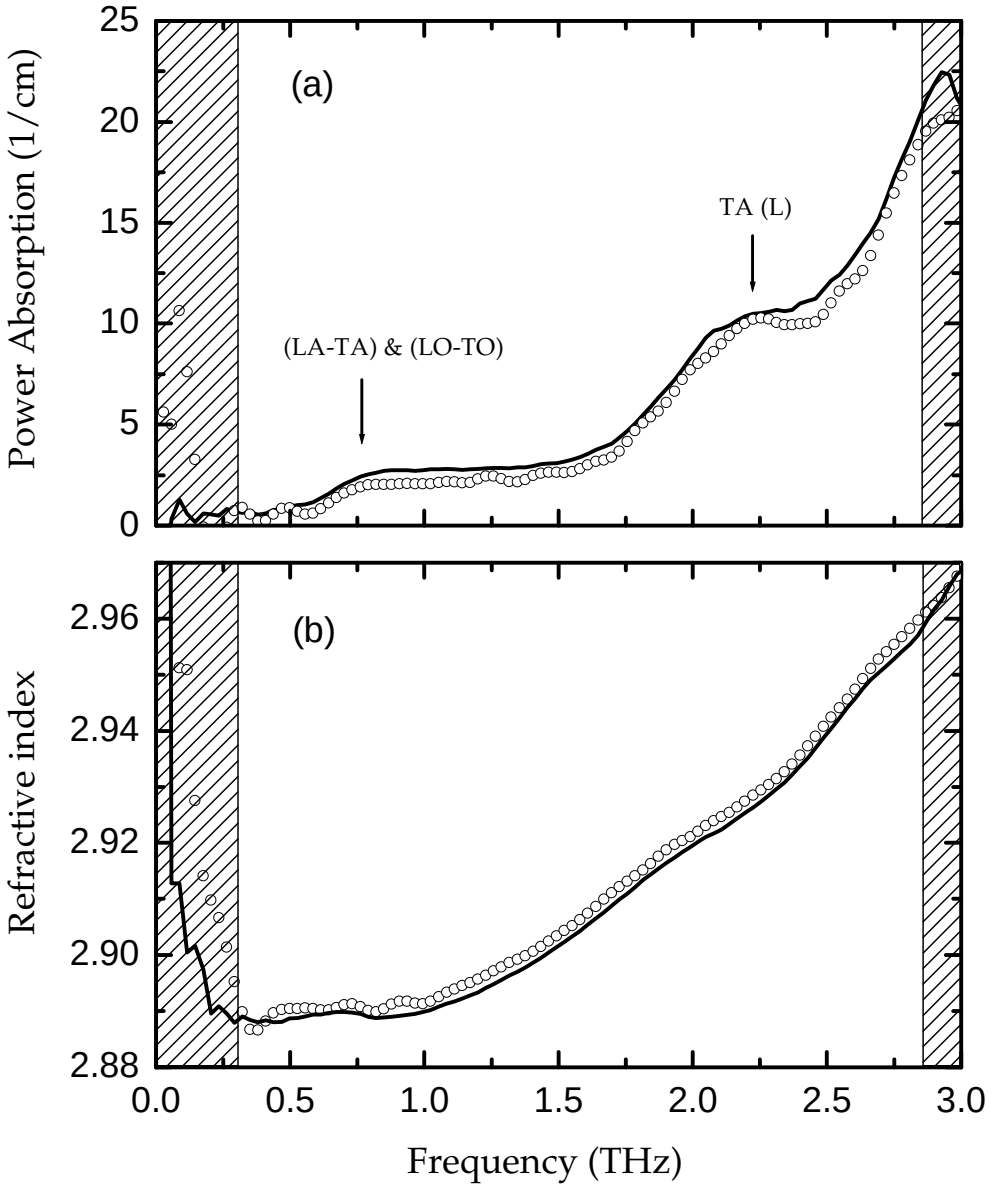

Figure 3-5 (a) Measured power absorption coefficient of polycrystalline ZnS (solid line) compared with that of single crystal ZnS (open circles). (b) Measured refractive index of polycrystalline ZnS (solid line) compared with that of single crystal ZnS (open circles).

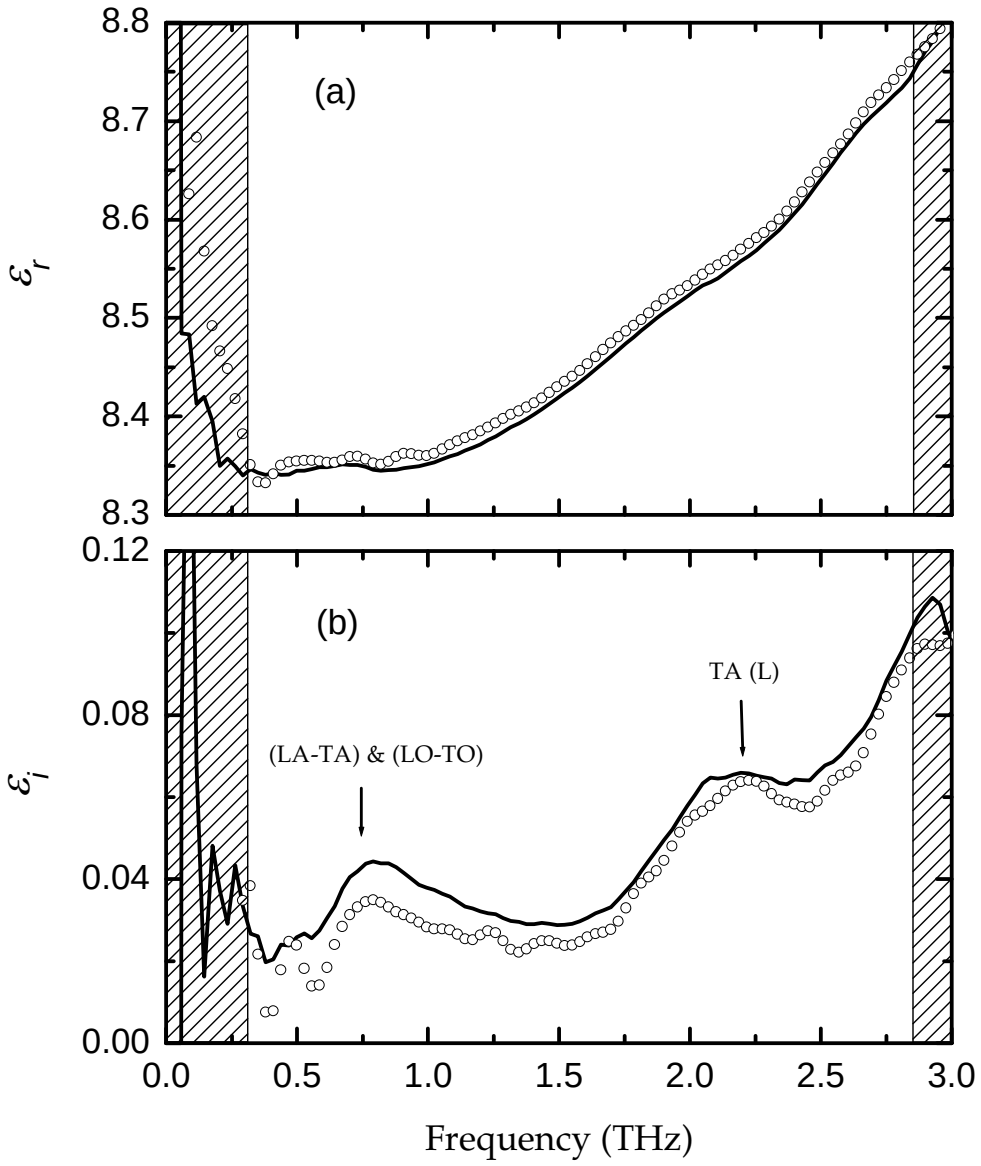

Figure 3-6 (a) Real dielectric constant of polycrystalline ZnS (solid line) compared with that of single crystal ZnS (open circles). (b) Imaginary dielectric constant of polycrystalline ZnS (solid line) compared with that of single crystal ZnS (open circles).

Figure 3-4 shows the measured sample pulse transmitted through polycrystalline ZnS, the reference pulse, and the corresponding Fourier amplitude spectra. In order to increase the S/N, seven individual measurements were averaged to obtain the curve of each pulse. The peak amplitude of the sample spectrum is reduced by about 58% due to the frequency-dependent absorption and reflection of the polycrystalline ZnS sample and other effects. Figure 3-5 shows the power absorption by polycrystalline ZnS and its refractive index compared with those of single crystal ZnS.

The measured data were analyzed using the same procedure as for single crystal ZnS previously mentioned and the power absorption and refractive index obtained. Figure 3-5 (a) shows the absorption spectrum of polycrystalline ZnS. Due to the high absorption at higher frequencies and the relatively thick (3.42 mm) sample, the accuracy of the measured power absorption coefficient of polycrystalline ZnS is limited to 2.9 THz. Compared with the measured data for single crystal ZnS (open circles), the power absorption coefficient of polycrystalline ZnS is slightly higher (figure 3-5 (a)), but shows the similar phonon peaks at 0.78 THz and 2.20 THz, respectively. In contrast, the measured refractive index of polycrystalline ZnS (solid line) shown in Fig. 3-5 (b) is slightly lower than that of single crystal ZnS (open circles). The frequency-dependent real and imaginary dielectric constant of polycrystalline ZnS are plotted in Fig. 3-6 as obtained from the application of the damped harmonic oscillator model. The real dielectric constant is nearly the square of the refractive index. The imaginary dielectric constant plot of polycrystalline ZnS

graphically outlines the phonon positions at 0.78 and 2.2 THz, similar to the case of single crystal ZnS.

The peaks in the absorption spectrum are observed at typical phonon frequencies, usually called infrared active vibrations [31]. Spectroscopic techniques, such as IR absorption, are used to map out the non-Raman active excitations which are usually infrared active [32].

CHAPTER IV

CHARACTERIZATION OF NANOPARTICLES OF ZnS

ZnS nanostructures acquire importance due to their sizes in the nanometer range. Numerous nanostructures such as nanobelts, nanorods and nanotubes have been produced which have prospective applications in the field of terahertz optoelectronics. This experiment is an attempt to further our understanding about semiconductor nanoparticles and their properties.

The sample used in this study consists of nanoparticles of ZnS each of size 3-5 nm. The frequency dependent dielectric properties were characterized by performing experiments using the THz- TDS setup described in the previous chapter.

4.1 Trials and improvements: Characterizing nanoparticles by suspending them in a liquid medium (toluene)

Characterization of nanoparticles of ZnS was attempted as follows. Nanoparticles of ZnS were suspended in a solution of toluene contained in rectangular, open top quartz cells with path length of 2 mm and outer dimensions 45mm x 12.5 mm x 4.5 mm (Starna Cells). The quartz cell was first filled with toluene and it acted as the reference. The THz

beam was allowed to pass through and toluene was characterized. The sample consisted of ZnS nanoparticles suspended in toluene. The THz beam was let to pass through and the ZnS particles were characterized. But measurements obtained this way were not very accurate for three reasons: first, the same cell had to be used as different cells might not give the same path length to the traveling beam. This meant that between successive scans of the reference and sample, the toluene in the cell had to be replaced by the ZnS solution. This process was cumbersome and some leftover ZnS particles from the solution contaminated the toluene to be used for the next scan. Second, if the concentration of the ZnS nanoparticles was too less (1.25 mg of ZnS/ ml of toluene), the obtained refractive index was too close to the refractive index of toluene and did not seem to reveal the properties of the nanoparticles of ZnS. Finally, if the solution concentration was too high (25.95 mg of ZnS/ml of toluene), it was difficult to keep the particles suspended. They formed a sediment at the bottom of the cell and again, did not characterize the ZnS in the solution. So, as an improvement, a glass syringe was used to keep disturbing the toluene solution so as to keep the ZnS nanoparticles suspended in it, at the same time, taking care not to interfere with the path of the terahertz beam. This approach did not prove very beneficial as the syringe got clogged with the ZnS particles.

4.2 Characterizing nanoparticles using silicon cells (no liquid medium)

Hand-made cells of silicon having a very small absorption coefficient and measuring 25mm x16 mm with a spacer thickness of 1 mm were employed. Two identical cells were used; the empty cell served as the reference and the other cell

contained the nanoparticles without using any solution. The results obtained from the characterization of the nanoparticles by THz- TDS using the previous mentioned setup are shown.

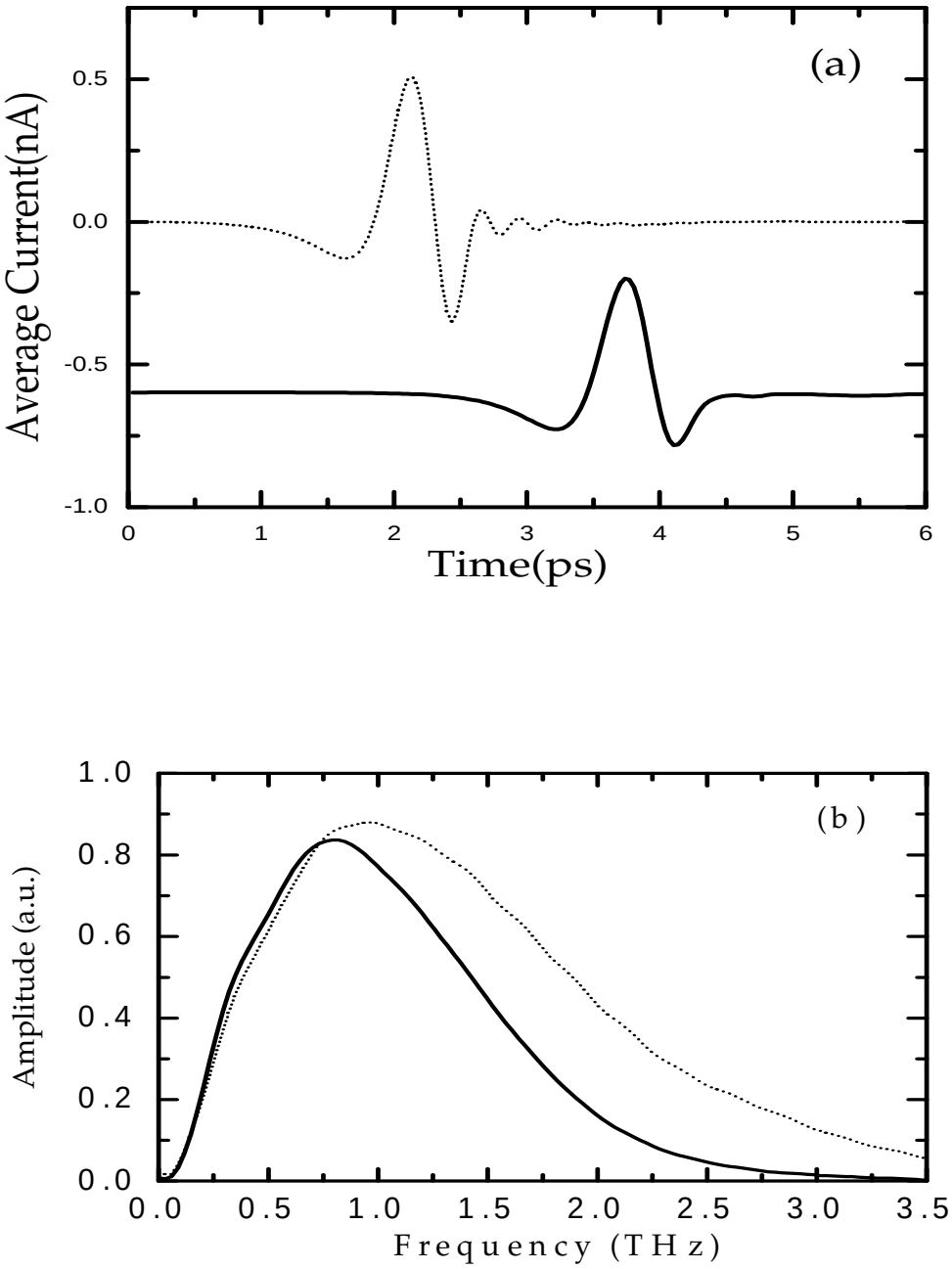

Figure 4-1 (a) Measured sample pulse transmitted through the ZnS nanoparticles (solid line offset by 0.6 nA for clarity) and the reference pulse (dotted line) and (b) the corresponding output (solid line) and reference (dotted line) Fourier amplitude spectra.

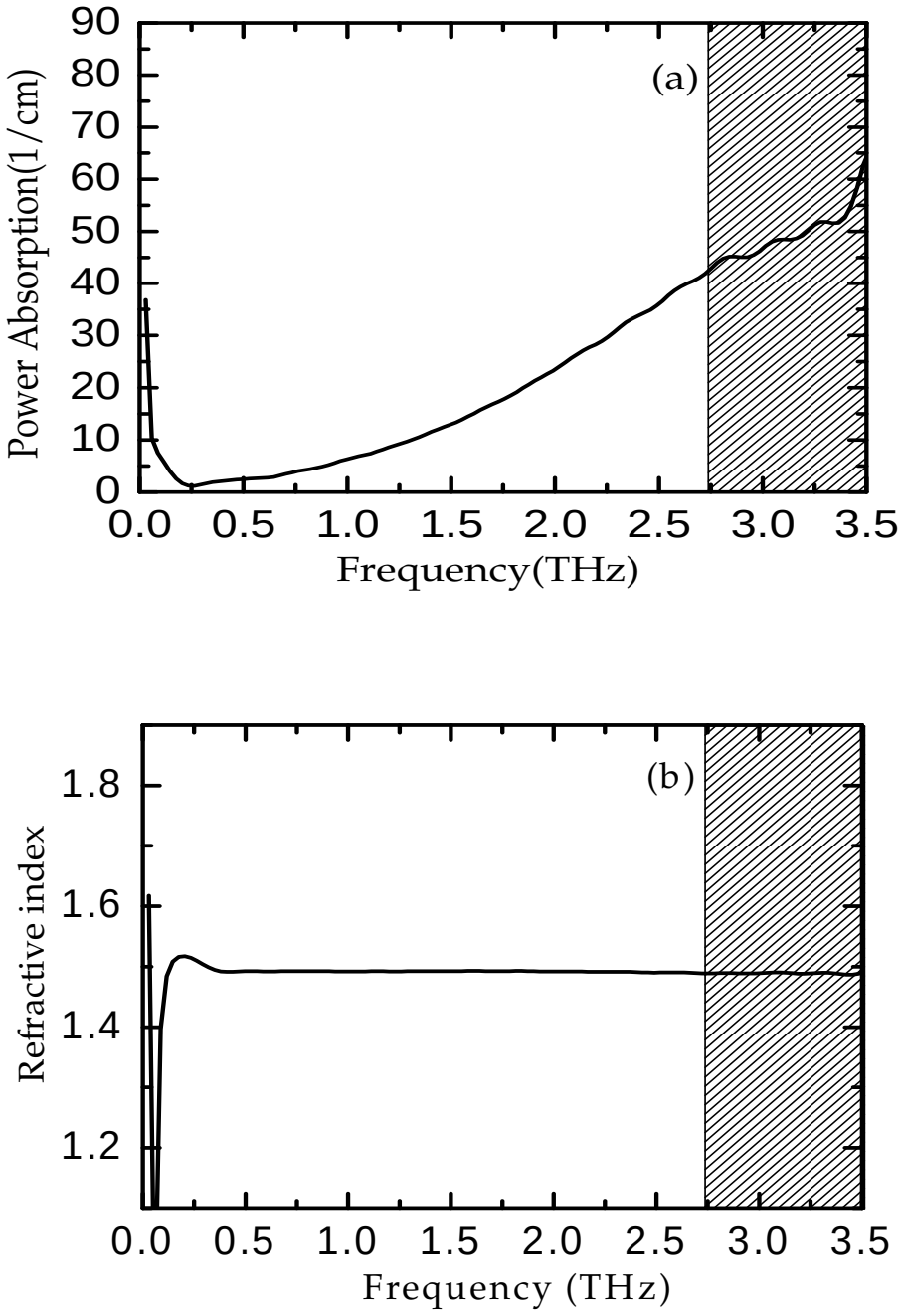

Figure 4-2 Measured (a) Absorption, and (b) Refractive index of composite medium of ZnS nanoparticles with air.

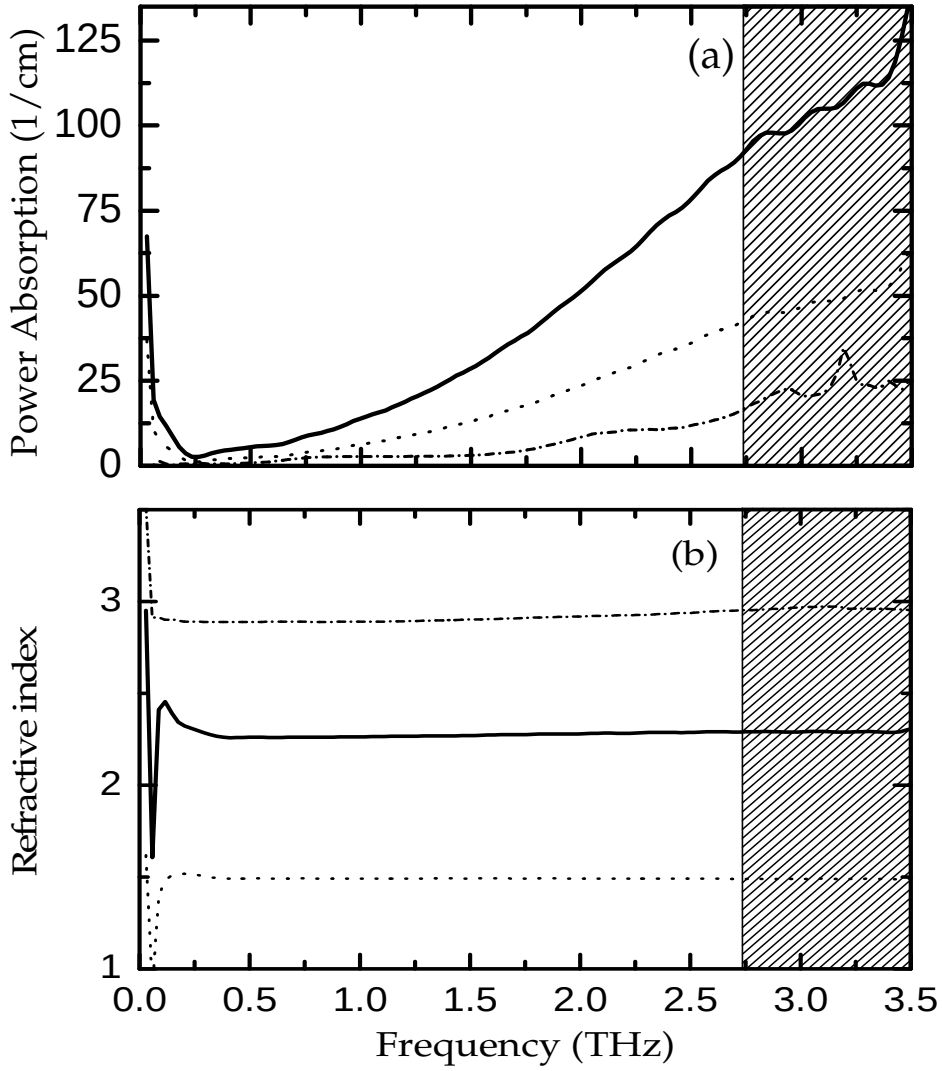

Figure 4-3 (a) Power absorption of ZnS nanoparticles (solid line) compared with that of a composite medium of ZnS nanoparticles in air (dotted line) and that of polycrystalline ZnS (short-dash-dotted line). (b) Refractive indices of nanoparticles of ZnS (solid line) compared with that of a composite medium of ZnS nanoparticles in air (dotted line) and that of polycrystalline ZnS (short-dash-dotted line).

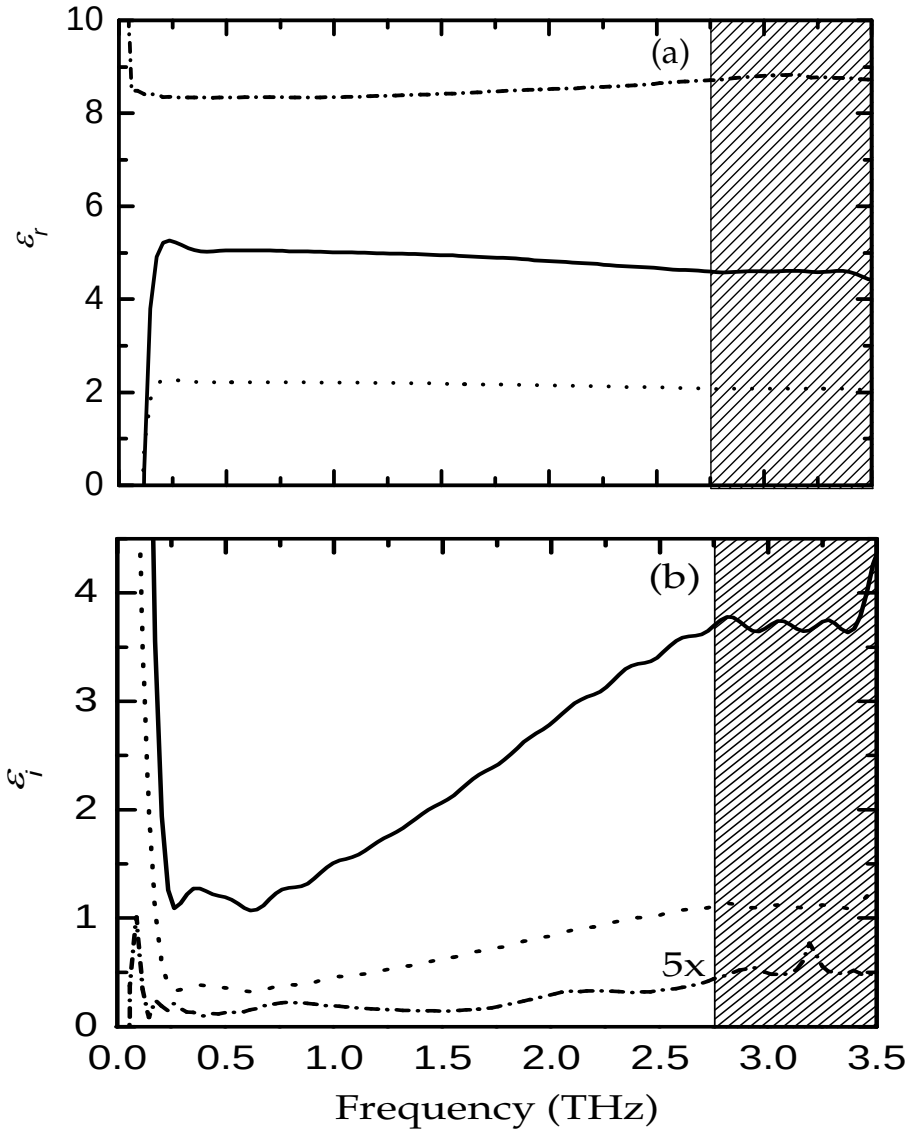

Figure 4-4 (a) Measured real part of dielectric constant ε_r, and (b) measured imaginary dielectric constant ε_i; a comparison of results between-nanoparticles of ZnS (solid line), composite medium of ZnS nanoparticles in air (dotted line) and polycrystalline ZnS (short-dash-dotted line); ε_i of polycrystalline ZnS has been scaled by a factor of 5 for clarity.

4.3 Experimental Results

Figure 4-1 shows the measured sample pulse transmitted through the ZnS nanoparticles in air, the reference pulse, and the corresponding Fourier amplitude spectra. In order to increase the S/N, six individual measurements were averaged to obtain the curve of each pulse. The peak amplitude of the sample spectrum is reduced by about 5% due to the frequency-dependent absorption and reflection of the ZnS nanoparticles in air and other effects. Figure 4-2 shows the power absorption and refractive index of the composite medium of ZnS nanoparticles with air.

The power absorption, refractive index and dielectric constants are measured as described previously with modifications made to include the effects of the silicon cell. The THz beam that enters the cell, suffers reflections at the front and back surfaces of the cell that have to be accounted for. A schematic diagram of the cell is shown in figure 4-5.

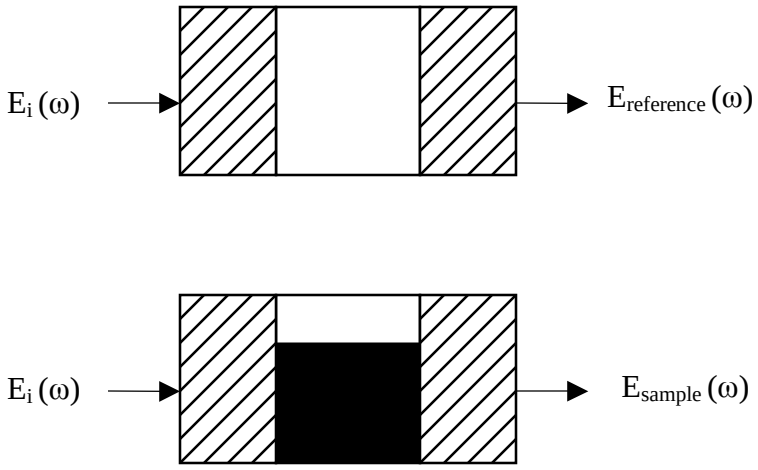

Figure 4-5 (a) Empty cell used as reference (b) Cell filled with nanoparticles to be characterized.

The transmission equations for the substrate-material arrangement are:

$$Ereference = E_{in} t_{sa} t_{as} exp\left(\frac{i2\pi n_a d}{\lambda}\right) \qquad (4-1)$$

$$Esample = E_{in} t_{sm} t_{ms} exp\left(\frac{i2\pi n_m d}{\lambda}\right) exp\left(\frac{-\alpha_m d}{2}\right) \qquad (4-2)$$

The refractive index is calculated from the total transmission function [14] of the air-substrate-material-substrate-air arrangement given by

$$z_t = \frac{t_{sm}\, t_{ms}}{t_{sa}\, t_{as}} \qquad (4\text{-}3)$$

where t_{sm} and t_{ms} are the transmission functions of the substrate-material and material-substrate interfaces and t_{sa} and t_{as} are the transmission functions of the sample-air and air-sample interfaces respectively. The Fresnel's coefficients are given by

$$t_{sm} = \frac{2n_s}{n_s + n_m}, t_{ms} = \frac{2n_m}{n_s + n_m}, tsa = \frac{2n_s}{1 + n_s}, tas = \frac{2}{1 + n_s} \qquad (4\text{-}4)$$

The effective volume of nanoparticles of ZnS when compressed so as to resemble bulk ZnS is approximately 30% of the original volume they occupied without compression. These are derived from the density of bulk ZnS which is 4.1 and the density of ZnS nanoparticles which is 1.3 as calculated from the mass - volume ratio (0.0644g of ZnS nanoparticles are contained in a cell of volume 0.0495 cm^3).

Figure 4-3 (a) shows the power absorption coefficient of nanoparticles of ZnS (solid line) compared with that of polycrystalline ZnS (short-dash-dotted line) and that of the measured composite medium of ZnS nanoparticles in air (dotted line). Figure 4-3 (b) shows the refractive index of nanoparticles of ZnS (solid line) compared with that of polycrystalline ZnS (short dash-dotted line) and that of the measured composite medium of ZnS nanoparticles in air (dotted line). Figure 4-3 (b) reveals that the refractive index obtained for the nanoparticles of ZnS is between than obtained for bulk ZnS and the composite medium.

4.4 Data Analysis

There is considerable difference between the values for the indices of refraction of the three cases in the frequency range under study. The index of refraction of the nanoparticles of ZnS is scaled to their density [28] using the relation between the two given by, $n = 1 + k\,\rho$ [28], where ρ is the density of the material, n is the refractive index and k is the scaling factor The coefficient of proportionality, k_{poly} is determined to be 0.46 from $n_{poly} = 1 + k_{poly}\rho_{poly}$ where, n_{poly} is 2.9 (as can be seen from Figure 3-5) and ρ_{poly} is 4.1 g/cm^3 (density of bulk ZnS). k_{nano} is similarly determined to be 0.38 using $n_{nano} = 1.5$ (as can be seen from Figure 4-2) and $\rho_{nano} = 1.3$ g/cm^3 (as determined from the mass-volume ratio). k_{nano} is thus estimated to be about 17% smaller than k_{poly} as determined from this formula. This observation is consistent with the results of silicon aerogels measured at both THz and optical frequency ranges [28,29].

The effective medium theory has been used to determine the optical and dielectric properties of the nanoparticles from the known properties of the constituents. Properties of the nanoparticles, roughly independent of the containing media and the interactions between each other have been found. The particle sizes for our case are large enough for the theory to work. The properties of the nanoparticles do not depend on the properties of bulk ZnS. Rather, they depend strongly on the effects due to the confinement of the electronic states [30].

The index and power absorption coefficient for the nanoparticles of ZnS are derived from the real and imaginary parts of the frequency-dependent dielectric function given by the simple mixing model [31]

$$\varepsilon(\omega) = f\varepsilon_{np}(\omega) + (1-f)\varepsilon_h(\omega) \qquad (4\text{-}5)$$

where the filling factor, f = 0.3 is the ratio of the volume of the ZnS nanoparticles to the volume of the cell that holds them. The dielectric function of the nanoparticles ε_{np}, is obtained from the dielectric function $\varepsilon(\omega)$ of the composite medium obtained by THz-TDS and from $\varepsilon_h(\omega)$ which is the dielectric constant of the host medium (air, in this case). The absorption spectrum depends on the size of the nanoparticles. The size in turn influences the confinement effects. The index value lies between that of the composite medium that is rarer (more air implies lesser index) and the denser bulk ZnS (index = 2.9).

Figure 4-4 shows the real and imaginary dielectric constants of ZnS nanoparticles of ZnS (solid line) compared with that of polycrystalline ZnS (short-dash-dotted line) and that of the composite medium of ZnS nanoparticles in air (dotted line).

The complex dielectric function for the composite medium is extracted from the frequency dependent absorption and refractive index using the formula of a damped harmonic oscillator mentioned previously while the simple mixing model was used to

evaluate the complex dielectric function of nanoparticles of ZnS. ε_r of the nanoparticles is smaller due to the strong absorption while ε_i is higher for the same reason.

CHAPTER V

CONCLUSIONS

In this study, a modified THz- TDS system was developed using an 8- F confocal system which was used to characterize different sample of ZnS. The arrangement utilizes a geometry that has four mirrors placed apart from each other by a distance that provides a tighter beam and a much more reduced waist than that obtained with the 4-F confocal system of two parabolic mirrors. Having such a collimated beam makes it easier for the entire beam to pass through samples with small dimensions such as the ones used for the experiments described in this thesis. The laser used is extremely stable and this method ensures increased accuracy as compared to other infrared approaches.

The material properties of ZnS have been studied. The refractive indices and absorption coefficients of single crystal and polycrystalline ZnS were found. The absorption spectra of the crystalline samples showed peaks that were assigned to TA phonons at 2.2 and 2.8 THz and the superposition of the two difference phonons, ((LO-TO)-(LA-TA)) at 0.78 THz. The refractive index we measured was lesser than the value from literature [1]. The curves for the index and absorption were fit using the damped harmonic oscillator model.

A comparison of our results with those published earlier is presented in table 6-1. The results obtained were in agreement with previous work.

Reference	TA(X) assignment cm^{-1}(THz)	TA(L) assignment cm^{-1}(THz)
Infrared spectrum[a] (Cubic ZnS)	88±1 (2.64- 2.7)	72±1 (2.15- 2.21)
Neutron scattering data[b] (zinc blende)	88 (2.67)	
Second- order Raman spectra[c] (cubic ZnS)	88 (2.67)	
Neutron data[d] (single crystal)	93- TA(L) (2.82)	73-TA(X) (2.21)
E2 mode[e] Raman- active phonon frequency(wurtzite type ZnS)		72 (2.18)
2H ZnS phonon frequency[f] E2- TA(L)		69.2 (2.10)
Phonon frequencies in hexagonal ZnS[g]	92 (2.79)	73 (2.21)
Multiphonon absorption band in cubic ZnS[h]	93 (2.82)	
Second neighbor ionic model (SNI) for cubic ZnS[i]	96 (2.91)	65 (1.97)

Table 6-1: Critical- point mode frequencies in cm^{-1} for ZnS at room temperature.

[a]From Table I in [1].

[b]From Table II in [17].

[c]From [21], pg. 182.

[d]From Ref 29 in [18].

[e]From [20], pg.933.

[f]From [22], pg.1293.

[g]From Table III in [17].

[h]From Table IV in [19].

[i]From [23].

The measured indices of refraction for the single crystal and polycrystalline ZnS were compared with the channel spectrum data and the theoretical fit, demonstrating that THz-TDS has the ability to determine optical and dielectric parameters more precisely than previous work.

Nanoparticles of ZnS were characterized by placing them in silicon cells. The refractive index obtained was lesser than the value for bulk and greater than the value of the composite medium while the absorption by the nanoparticles was much larger than that of nanoparticles of ZnS in air and that of bulk ZnS.

CHAPTER VI

REFERENCES

1. T. Hattori, Y. Homma, A. Mitsuishi, and M. Tacke, Opt. Commun. **7**, 229 (1973).
2. B. Y. Geng, L. D. Zhang, G. Z. Wang, T. Xie, Y. G. Zhang, and G. W. Meng, Appl. Phys. Lett. 84, 2157 (2004).
3. S. Gupta, J. S. Meclure, and V. P. Singh, Thin Solid Films 33, 299 (1997).
4. Y. Jiang, X. M. Meng, J. Liu, Z. Y. Xie, C.-S. Lee, and S. T. Lee, Adv. Mater. (Weinheim, Ger.) 15, 323 (2003).
5. X. M. Meng, Y. Jiang, J. Liu, C.S .Lee, I. Bello and S.T. Lee, Appl. Phys. Lett. 83, 11 (2003).
6. Y. Jiang, X. M. Meng, C. S. Lee, and S. T. Lee, Adv. Mater. (Weinheim,Ger.) (to be published).
7. Y. C. Zhu, Y. Bando, and Y. Uemura, Can. Ceram. Q. 7, 836 (2003).
8. A. K. Verna, T. B. Ranchfuss, and S. R. Wilson, Inorg. Chem. **34**, 3072 (1995).
9. T. Sugimoto, S. Chen, and A. Muramatsu, Colloids Surf., A **135**, 207 (1998).
10. Tae- In Jeon and D. Grischowsky, Appl. Phys. Lett., Vol. 72, 3032-3034 (1998).
11. G. Gallot, J. Zhang, R. W. McGowan, T. I. Jeon, and D. Grischkowsky, Appl. Phys. Lett. **74**, 3450 (1999).
12. H. J. Bakker, G. C. Cho, H. Kurz, Q. Wu, and X. –C. Zhang, J. Opt. Soc. Am. B **15**,

1795 (1998).

13. Orazio Svelto, Principle of Lasers , 4th ed. (Plenum Press, New York, 1998) p- 148-154.
14. M. Born, and E. Wolf, Principles of Optics, 7th (expanded) ed. (Cambridge University Press, Cambridge, UK, 2002), p. 65, Eq. (58).
15. R. Marshall and S.S. Mitra, Phys. Rev. 134, A1019-1025 (1964).
16. G. A. Slack and S. Roberts, Phys. Rev. **3**, 2615 (1971).
17. N. Vagelatos, D. Wehe, and J. S. King, J. Chem. Physics **60**, 3613 (1974).
18. O. Brafman and S.S. Mitra, Phys. Rev. 171, 931- 934 (1968).
19. H. Poulet, W.E. Klee and J.P. Mathieu, in Proceedings of the International Conference on lattice Dynamics, Copenhagen, 1963 (Pergamon Press, Inc., New York, 1965), pp. 337-341.
20. J. Scheinder and R.D. Kirby, Phy. Rev. B, 6, 1290- 1294 (1972).
21. W.G. Nilsen, Phys. Rev., 182, 838-850(1969).
22. J.C. Irwin, Canadian journal of physics, 48, 2477- 2480 (1970).
23. C. A. Klein, and R. N. Donadio, J. Appl. Phys. **51**, 797 (1980).
24. Y. V. Korostelin, V. I. Kozlovsky, A. S. Nasibov, P. V. Shapkin, S. K. Lee, S. S. Park, J. Y. Han, and S. H. Lee, J. Crystal Growth **184/185**, 1011 (1998).
24. W. Zhang, A. K. Azad, and D. Grischkowsky, Appl. Phy. Lett. **82**, 2841 (2003).
25. L. A. Feldkamp, G. Venkataraman, and J. S. King, Solid State Commun. **7**, 1571 (1969). J. Bergsma, Phys. Lett. **32A**, 374 (1970).
26. Lin-Wang Wang, and Alex Zunger, Phys.Rev.Lett. 73, 1039 (1994).
27. K. M. Yeung, W. S. Tsang, C. L. Mak, and K. H. Wong, J. Appl. Phys. 92, 3636

(2002).

28. Zhang et al. “THz Time-Domain Spectroscopy on Silica Areogels” (to be published).
29. Buzykaev, A.R.; Danilyuk, A.F.; Ganzhur, S.F.; Kravchenko, E.A.; Onuchin A.P, “ Measurement of optical parameters of areogel”, Nucl. Instr. And Meth.A 1999, 433, 396.
30. H.-Ch.Weissker, J.Furthmuller and F.Bechstedt, Phys. Rev. B 67, 165332 (2003).
31. Fratini and F. de Pasquale, Phys. Rev. B, 63, 153101.
32. http://physics.nist.gov/Divisions/Div844/facilities/raman/Ramanhome.html

APPENDIX

Derivation of refractive index (*n*) and absorption coefficient (*k*) from frequency dependent dielectric constant of a damped harmonic oscillator.

The complex dielectric constant of a damped harmonic oscillator can be represented as

$$\varepsilon(\Omega) = \varepsilon_{el} + \frac{\varepsilon_{st}\Omega_{TO}^{2}}{\Omega_{TO}^{2} - \Omega^{2} + 2i\gamma\Omega} = (n + ik)^2 \qquad \text{(A-1)}$$

where

$\varepsilon(\Omega)$ is the frequency- dependent complex dielectric constant

ε_{el} is the optical dielectric constant

ε_{st} is the strength of the TO phonon resonance at $\Omega_{TO}/2\pi$

Ω_{TO} is the TO phonon frequency

Ω is the angular frequency

γ is the linewidth of resonance

Multiplying and dividing the second term on the left hand side of equation (A-1) by its complex conjugate and expressing the equation as a combination of real and imaginary parts, we get

$$\varepsilon(\Omega) = \varepsilon_{el} + \frac{\varepsilon_{st}\Omega_{TO}{}^2(\Omega_{TO}{}^2 - \Omega^2)}{(\Omega_{TO}{}^2 - \Omega^2) + 4\gamma^2\Omega^2} - \frac{\varepsilon_{st}\Omega_{TO}{}^2(2i\gamma\Omega)}{(\Omega_{TO}{}^2 - \Omega^2) + 4\gamma^2\Omega^2} \quad \text{(A-2)}$$

Expanding the right hand side of equation (A-1) and separating it into real and imaginary parts, we get

$$(n + ik)^2 = n^2 - k^2 + 2ink \quad \text{(A-3)}$$

Equating the real parts of equation (A-2) with those of equation (A-3) and the imaginary parts of equation (A-2) with those of equation (A-3) we get

$$n^2 - k^2 = \varepsilon_{el} + \frac{\varepsilon_{st}\Omega_{TO}{}^2(\Omega_{TO}{}^2 - \Omega^2)}{(\Omega_{TO}{}^2 - \Omega^2) + 4\gamma^2\Omega^2} \quad \text{(A-4)}$$

$$2nk = \frac{-2\gamma\Omega(\varepsilon_{st}\Omega_{TO}{}^2)}{(\Omega_{TO}{}^2 - \Omega^2)^2 + 4\gamma^2\Omega^2} \quad \text{(A-5)}$$

Solving for '*n*' in terms of '*k*' we get

$$n = \frac{-\gamma\Omega(\varepsilon_{st}\Omega_{TO}{}^2)}{k[(\Omega_{TO}{}^2 - \Omega^2)^2 + 4\gamma^2\Omega^2)]} \quad \text{(A-6)}$$

Substituting (A-6) in (A-4) we get

$$\frac{\gamma\Omega(\varepsilon_{st}\Omega_{TO}{}^2)^2}{k^2((\Omega_{TO}{}^2 - \Omega^2)^2 + 4\gamma^2\Omega^2)^2} - k^2 = \varepsilon_{el} + \frac{\varepsilon_{st}\Omega_{TO}{}^2(\Omega_{TO}{}^2 - \Omega^2)}{(\Omega_{TO}{}^2 - \Omega^2) + 4\gamma^2\Omega^2} \quad \text{(A-7)}$$

Let

$$\frac{\gamma\Omega(\varepsilon_{st}\Omega_{TO}{}^2)^2}{((\Omega_{TO}{}^2 - \Omega^2)^2 + 4\gamma^2\Omega^2)^2} = y$$

$$k^2 = x$$

$$\varepsilon_{el} + \frac{\varepsilon_{st}\Omega_{TO}{}^2(\Omega_{TO}{}^2 - \Omega^2)}{(\Omega_{TO}{}^2 - \Omega^2) + 4\gamma^2\Omega^2} = z$$

Substituting y, x and z in equation (A-7) we get a simple quadratic equation in terms of x,

$$\frac{y}{x} - x = z \Rightarrow x^2 + zx - y = 0$$

Solving this equation we get

$$k = \sqrt{x} = \sqrt{\frac{-z \pm \sqrt{z^2 + 4y}}{2}} \qquad \text{(A-8)}$$

'*n*' can be obtained from equation (A-6) after finding '*k*' from equation (A-8) and substituting it back in equation (A-6).

VITA

Lakshmi Thamizhmani

Candidate for the Degree of

Master of Science

Thesis: MEASUREMENTS OF THE DIELECTRIC PROPERTIES OF ZnS IN THE FAR INFRARED USING THz- TDS

Major Field: Electrical Engineering

Biographical:

Personal Data: Born in Chennai, Tamil Nadu, India on 19th December 1981, the daughter of T. Thamizhmani and G. Mangalam.

Education: Graduated from Padma Seshadri Bala Bhavan Senior Secondary School, Chennai, Tamil Nadu, India in April 1996, received a Bachelor's Degree in Electronics and Communication Engineering from the University of Madras, Chennai, India in June 2002, completed the requirements for the Masters Degree in Electrical Engineering at Oklahoma State University in December 2004.

Experience: Employed by OSU, School of Electrical and Computer Engineering, as a teaching assistant from August 2003 to December 2004 and as a research assistant from May 2004 to present.

Professional Membership: Institute of Electrical and Electronics Engineers.

Name: Lakshmi Thamizhmani **Date of Degree**: December, 2004

Institution: Oklahoma State University **Location**: Stillwater, Oklahoma

Title of Study: MEASUREMENTS OF THE DIELECTRIC PROPERTIES OF ZnS IN THE FAR INFRARED USING THz- TDS

Pages in Study: 60 Candidate for the Degree of Master of Science

Major Field: Electrical Engineering

Scope and Method of Study: The purpose of this study was to characterize the frequency dependent optical and dielectric properties of ZnS in the far infrared region by using the highly precise method of THz time domain spectroscopy. Single crystal, polycrystalline and nanoparticles of ZnS were characterized. The experimentally determined, frequency- dependent power absorption coefficients and refractive indices of the crystalline ZnS samples were fit using the damped harmonic oscillator model while the simple mixing model was used to determine the corresponding values for nanoparticles of ZnS.

Findings and Conclusions: The experimental results for the absorption coefficient and refractive index of crystalline ZnS fit well with the published results. It is observed that the absorption in both the single- and poly-crystalline ZnS is characterized by prominent acoustic phonons which account for the increased absorption as indicated by the resonance lines in the spectra. At a low frequency, superposition of difference phonons was also observed. The measured index of refraction of the crystalline samples is found to be dominated by the TO-phonon resonance which is verified by a theoretical fit using the relation for the dielectric response of the damped harmonic oscillator. The frequency dependent optical properties of the nanoparticles of ZnS were found using the simple mixing model which revealed that the large absorption by nanoparticles is attributed to confinement effects and the refractive index is related to the density of nanoparticles.

Advisor's Approval Weili Zhang